Quantitative theory of diffraction by carbon nanotubes

Ph. Lambin and A. A. Lucas
Département de Physique, Facultés Universitaires Notre-Dame de la Paix, 61 Rue de Bruxelles, B-5000 Namur, Belgium
(Received 15 April 1997)

A quantitative theory of the kinematical diffraction of a plane wave by a carbon nanotube is developed. The formalism is based on the Cochran, Crick, and Vand theory of the diffraction by helical molecules. This leads to a closed-form expression of the diffracted amplitude produced by a single-wall tubule of arbitrary helicity, applicable to both X rays and high-energy electrons. The theory, which can be used to simulate the diffraction pattern of any multilayer nanotube, is illustrated on the case of a crystalline rope of carbon nanotubes. [S0163-1829(97)03631-X]

The investigation of the diverse physical properties of carbon nanotubes, as well as the prospect of their potential technological use are intense fields of current research.[1,2] A complete characterization of a multiwall nanotube would be achieved by sequencing the chiral vectors (L,M) of the successive layers, but determining these helical parameters remains a challenge, even for single-wall tubules packed in crystalline ropes.[3–5] High-resolution transmission electron microscopy (TEM) is the most direct way of measuring the geometrical parameters of a nanotube.[6–9] However, only in certain favorable circumstances can the helicities of the tubule layers be estimated by TEM,[10] and this becomes almost impossible with single-wall tubules.

Geometrical constructions in the reciprocal space show that the helicity of a single-wall nanotube can in principle be read directly from the diffraction pattern it produces.[11,12] In this geometrical interpretation, the presence or absence of intensity in a given diffraction direction is discussed in terms of the corresponding pattern of a flat graphite network suitably rolled up into a circular cylinder. The kinematical theory of plane wave diffraction by a nanotube, which is the subject of the present report, can be used to predict the relative intensities of the diffraction spots, and this should certainly help with the interpretation of experimental data.

Given that a carbon nanotube can be constructed with a finite set of helices, the diffraction patterns produced can be calculated[13,14] by the application of the CCV theory developed by Cochran, Crick, and Vand to account for the x-ray pictures of biological helical molecules.[15] The diffraction intensities computed from a first implementation of this theory[14] for a seven-layer nanotube was found in good agreement with the observations.[6] In the present paper the intensities of diffraction spots produced by a carbon nanotube are derived in a more complete formulation than in Ref. 14. Generalizations of the present formalism to BCN and metal dichalcogenides nanotubes[16] are straightforward.

Most generally, a carbon nanotube is composed of several concentric, single-wall tubules whose radii increase by steps of 0.34 nm. The first Born approximation simply needs adding the complex amplitudes of the waves scattered by the successive layers, and these are given by

$$S(\vec{k}) = f(\vec{k}) \sum_j \exp(i\vec{k}\cdot\vec{r}_j), \tag{1}$$

where $\vec{k}$ is the wave-vector transfer, $f(\vec{k})$ is the atomic form factor of carbon, and the sum runs over the atomic coordinates. The intensity of the wave diffracted in the direction specified by $\vec{k}$ is the square modulus of $S(\vec{k})$. It will prove useful in the following to decompose $\vec{k}$ into its components $\vec{k}_\perp$ and k_z, respectively, perpendicular and parallel to the tubule axis, and specifying the azimuth angle ϕ_k of $\vec{k}_\perp$ in the (x,y) plane.

A tubule is characterized by the two components L and M of its wrapping vector on the honeycomb lattice, where $L>0$ and $-L/2 \leqslant M \leqslant L$.[17] The (L,M) tubule with $M \geqslant 0$ (respectively, $M<0$) can be viewed as composed of L (respectively, $L-|M|$) pairs of right-handed (respectively, left-handed) helices which project along zig-zag carbon chains on the planar development of the structure (see Fig. 1). Let us first consider the structure factor of a monoatomic, right-handed helix as obtained from the CCV theory. The result is[18]

$$S(\vec{k}) = f(\vec{k}) \ \frac{2\pi}{p_z} \sum_{n,m} J_n(k_\perp r) e^{in(\phi_k - \phi_0 + \pi/2)} e^{ik_z z_0} \times \delta(k_z - n2\pi/P - m2\pi/p_z). \tag{2}$$

In Eq. (2), J_n is the cylindric Bessel function of order n, r is the tubule radius, ϕ_0 and z_0 are the azimuth angle and axial position of a reference site of the helix, p_z is the distance along z between two successive sites of the helix of which P is the pitch. These latter two quantities are related to the geometrical parameters C (circumference $2\pi r$) and α (chiral angle indicated in Fig. 1) of the tubule through $P = C/\tan(\pi/6+\alpha)$ and $p_z = a\cos(\pi/6+\alpha)$, with a the lattice parameter of graphite. P and p_z are always commensurate so that $n/P + m/p_z = l/T$, with l an integer and T, the least common multiple of P and p_z, is the true period of the helix. As a result, the diffraction pattern of a single such helix in the reciprocal space is composed of equidistant planes normal to the z axis:

$$S(\vec{k}) = f(\vec{k}) \sum_l s_l(\vec{k})\, \delta(k_z - l2\pi/T), \tag{3}$$

where

 © 1997 The American Physical Society

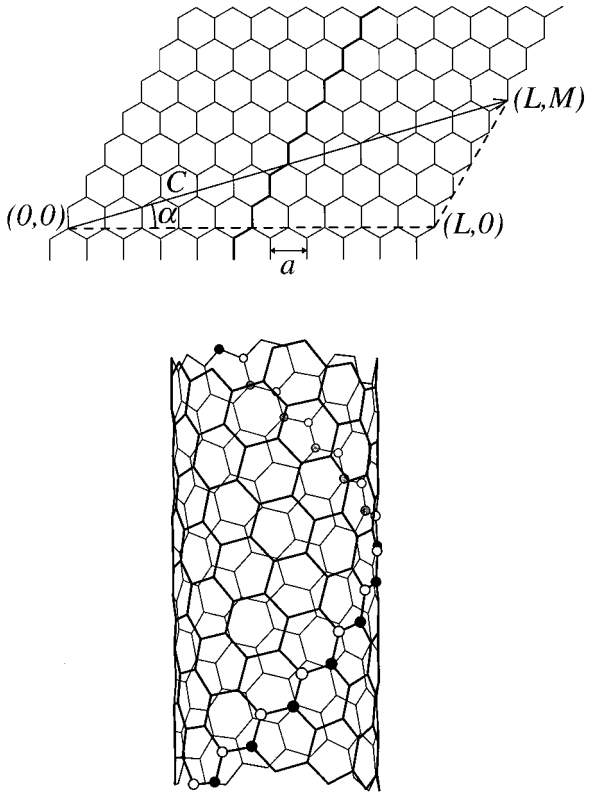

FIG. 1. The zig-zag chain visualized by thicker lines in the planar development (top) becomes a helix on the rolled-up structure (bottom) illustrated here for the (10,4) tubule. The helix is decomposed into two monoatomic helices (open and black circles) and ten pairs of such helices are used to construct the full structure of the nanotube.

$$s_l(\vec{k}) = e^{il2\pi z_0/T} \frac{2\pi}{p_z} \sum_{m,n} J_n(k_\perp r) e^{in(\phi_k - \phi_0 + \pi/2)} \times \delta_{nT/P + mT/p_z, l}. \quad (4)$$

The structure factor of the second helix that makes a pair is obtained from Eq. (4) by translating the reference site from (ϕ_0, z_0) to $[\phi_0 + (2\pi/C)d\sin\alpha,\ z_0 + d\cos\alpha]$, with $d = a/\sqrt{3}$ being the C-C nearest-neighbor distance. Still assuming $M \geqslant 0$, the L pairs of helices which the (L,M) tubule is made from correspond to one another by application of a rotation $\Delta\phi = (2\pi/C)a\cos\alpha$ and a translation $\Delta z = -a\sin\alpha$. Adding the structure factors of all these helices leads after some algebra to

$$s_l(\vec{k}) = e^{il2\pi z_0/T} \frac{2\pi}{p_z} \sum_{m,n} J_n(k_\perp r) e^{in(\phi_k - \phi_0 + \pi/2)} \delta_{nT/P + mT/p_z, l} \times (1 + e^{i2\pi\{[n + (2L+M)m]3L\}}) \sum_{j=0}^{L-1} e^{ij2\pi[(n+mM)/L]}. \quad (5)$$

Clearly the last factor of this equation is zero, unless $n + mM = sL$ with s an integer. This condition combined with $l/T = n/P + m/p_z$ implies $l/T = s(L+2M)/\sqrt{3}C + m(2L+M)/\sqrt{3}C$ after P and p_z have been replaced by their expressions. From this, T can be set to the true Bravais period of the tubule[19] $T = \sqrt{3}C/N$ with N = h.c.d. $(2L+M, 2M+L)$, and the layer-line index l must satisfy the selection rule $l = s(L+2M)/N + m(2L+M)/N$ where s and m are two integers. The layer-line structure of the diffraction pattern is the consequence of the honeycomb lattice having a well-defined parameter in the direction parallel to the tubule axis. In the direction perpendicular to the axis, the lattice parameter seen by the electrons decreases from the center towards the edges of the tubule, as a consequence of curvature. For these reasons, the diffraction spots are sharply defined along z but are elongated in the perpendicular direction. The $J_n(k_\perp r)$ Bessel function gives rise to a first maximum of intensity at $k_\perp \sim n/r$, followed by secondary maxima with decreasing intensities away from the tubule axis.

The (L,M) tubule with a negative M is equivalent to the $(L+M, -M)$ one, except for the handedness which changes from left to right. Exploiting this relation allows one to generalize the above results to all cases. The amplitude along the lth layer line of the wave diffracted by a single-wall (L,M) tubule, as defined in Eq. (3), is as follows:

$$s_l(\vec{k}) = e^{il2\pi z_0/T} \frac{4\pi C}{\sqrt{3}a^2} \sum_{s,m} J_{sL' - mM'}(k_\perp r) \times e^{i(sL' - mM')(\sigma\phi_k - \sigma\phi_0 + \pi/2)} (1 + e^{i(2\pi/3)(s+2m)}) \times \delta_{s(L'+2M')/N + m(2L'+M')/N, l}, \quad (6)$$

where $L' = L$, $M' = M$, $\sigma = +1$ when $M \geqslant 0$, and $L' = L + M$, $M' = -M$, $\sigma = -1$ when $M < 0$, and

$$T = \frac{\sqrt{3}C}{N}, \quad (7)$$

$$N = \text{h.c.d.}(2L' + M', 2M' + L'), \quad (8)$$

$$C = a\sqrt{L^2 + M^2 + LM}. \quad (9)$$

The two terms in the factor $(1 + e^{i2\pi(s+2m)/3})$ in Eq. (6) come from the two carbons that compose the diatomic helix shown in Fig. 1. For a BN nanotube, one simply needs to multiply these two terms by the atomic factors of the B and N atoms [and remove the prefactor $f(\vec{k})$ from the front of the Eq. (3)]. This already shows that BN and C nanotubes have the same diffraction pattern, except for possible small variations of the intensities. Note that the small buckling of the bonds predicted for BN nanotubes[20] can be taken into account by giving different radii to the B and N helices.

The diffraction pattern produced by an arbitrary collection of oriented single-wall tubules can be simulated on the computer by summing the amplitudes $S_I(\vec{k})$ of the individual tubules $(I = 1 \cdots N)$ multiplied by the phase factors $\exp(i\vec{k}_\perp \cdot \vec{\rho}_I)$ arising from the positions of their axes in the (x,y) plane, and by giving appropriate values to the coordinates of the origin atom $\vec{r}_0 I$ of each tubule. The diffraction intensity is the square of the modulus of the complex amplitude so obtained. This of course includes the case of a multilayer nanotube for which all the $\vec{\rho}_I$'s take the same value.

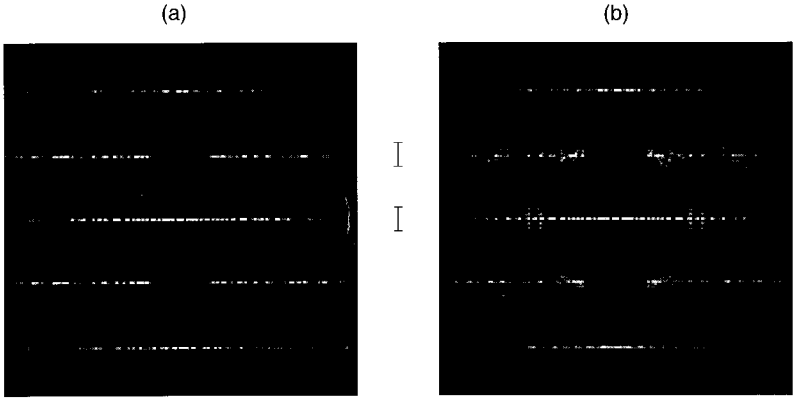

FIG. 2. Diffraction intensities computed for a crystalline rope of 37 single-wall carbon nanotubes (one nanotube surrounded by three shells of 6, 12, and 18 nanotubes). The intensities were saturated so as to reveal weak features. All the nanotubes in (a) were (10,10) nonchiral tubules. The rope (b) was a random mixture of 18 (10,10), 11 (11,9), and 8 (12,8) tubules. In both cases, the diffraction wave vector varied from 0 (at the center) to 7.0 Å^{-1} along the N, S, W, and E directions, with the S-N line parallel to the axis of the nanotubes.

As an application of this formalism, we have computed the diffraction pattern produced by a close-packed array of 37 single-wall nanotubes, for which we used the two-dimensional lattice parameter $a_h = 1.695$ nm measured recently in the ropes produced by laser ablation of graphite.[3] No coherence was assumed between the neighboring nanotubes: The coordinates ϕ_0 and z_0 of the reference atoms in the tubules were chosen at random. The diffraction patterns shown in Fig. 2 were computed using the atomic form factor of C for electrons given in the literature.[21] The electron beam, which we supposed much larger then the diameter (10 nm) of the rope, was taken normal to the nanotube axes, along a [100] direction of the rope. Figure 2(a) shows the intensity obtained for a homogeneous system composed exclusively of (10,10) nanotubes. The central, horizontal line is the $l=0$ layer line, dominated at the center by a J_0 Bessel function. Above and below the central line are the $l=\pm 1$ layer lines, dominated by $J_{\pm 10}$ whose principal maxima are positioned at 1 and 11 o'clock from the center of the image. Next come the $l=\pm 2$ lines on the top and the bottom of the image. In Fig. 2(b) the rope was a random mixture of (10,10), (11,9), and (12,8) single-wall nanotubes, with approximate proportions 5:3:2.[5] The most important effect of mixing the nanotubes is a somewhat diffuse structure of the layer lines which is due to the coexistence of three helicities.

In order to compare the calculations with available x-ray diffraction (XRD) data, the intensities were plotted against the modulus of the exchanged wave vector $k=4\pi\sin\theta/\lambda$, using the appropriate atomic factor[21] of C. Figure 3 shows the diffraction profiles scanned in the regions indicated by the vertical bars in Fig. 2 around (a) $k_z = 0$—the central-layer line—and (b) $k_z=2\pi/a$—the first-layer line of the (10,10) nanotubes. The diffraction intensity of the inhomogeneous rope has been represented with positive values in Fig. 3 where it is compared to that of the homogeneous rope represented with negative values. In both regions (a) and (b), there is not much difference between the two ropes, meaning that it would be hard to decide the actual composition of the rope from raw XRD profiles.

The dashed curves in Fig. 3 show the x-ray profile of a single (11,9) nanotube (positive ordinates) and that of a single (10,10) nanotube (negative ordinates) in the central (a) region. By comparison, the diffraction profiles of the ropes are hatched by the rapidly oscillating structure factor of the two-dimensional close-packed array. With the Cu Kα wavelength (1.5406 Å) used in the calculations, and for the assumed [100] incidence direction, the rope has two intense Bragg spots occuring in region (a) at $k = 0.43$ and 3.00 Å^{-1}. The first spot, (0,1), is undoubtedly present in the experimental XRD data and the second might mix with a broad structure at 3.1 Å^{-1} attributed to Co-Ni (100).[3] It is this

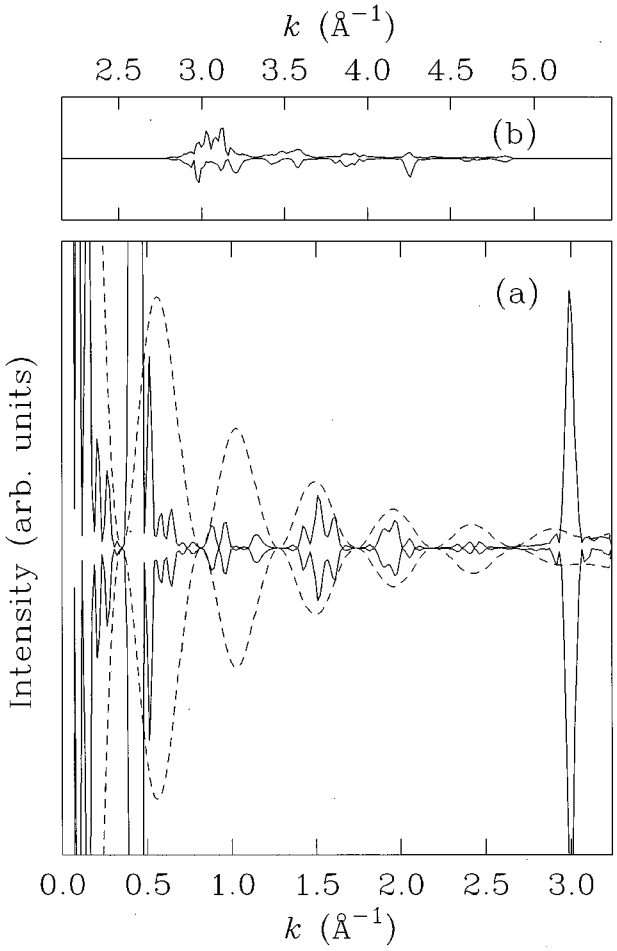

FIG. 3. Scan of the diffraction intensities in two k_z interval around (a) $k_z = 0.0$ and (b) $k_z = 2.55$ Å^{-1} indicated by the vertical bars between Fig. 2(a) and Fig. 2(b), and plotted against $|\vec{k}|$. Negative (respectively, positive) ordinates have been used for the rope made of 37 (10,10) nanotubes [respectively, the random mixing of (10,10), (11,9), and (12,8) tubules]. The dashed curves show the diffraction profile of a single (10,10) (negative ordinates) and (11,9) (positive ordinates) nanotube.

latter Bragg spot of the rope, $(5,-3)$, that is responsible for the peaks at $k = 3$ Å^{-1} in Fig. 3(a). An isolated (10,10) nanotube has more intensity there than the (11,9) or (12,8) chiral tubules because of positive interferences between the dominant J_0 Bessel function and the emerging J_{20} function. This explains why the peak at 3 Å^{-1} is more intense for the homogeneous rope than for the mixed system. Indeed the $l=0$ line of the chiral tubules is only composed of J_0 (at least for any reasonable k). The J_{20} function arises in the $l=\pm 1$ lines and yields the weak spots immediately above and below the central line in Fig. 2(b). As a consequence their intensities simply add together when scanning the region (a). By contrast, the positive interference realized in the $l=0$ line of the armchair (10,10) nanotube yields an intensity larger than the simple sum of the individual intensities set up by the J_0 and J_{20} functions.

To conclude, there are only weak differences between the diffraction pattern of an homogeneous rope of (10,10) single-wall nanotubes and the one produced by mixing (10,10), (11,9) and (12,8) tubules, which all have about the same diameter. Nevertheless, differences of that sort have been emphasized by nanodiffraction experiments across a rope that probe small amount of nanotubes.[5] The intensity of Bragg spots probing the central-layer line near $k = 3$ Å^{-1} could reveal the proportion of armchair nanotubes.

It is a pleasure to thank Professor S. Amelinckx and D. Bernaerts for many discussions and for their constant interest in this work. This work has been performed under the auspices of the Belgian State Interuniversity Research Program on reduced dimensionality systems (PAI/IUAP No 4/10).

[1] M. S. Dresselhaus, Phys. World **9**, 18 (1996).
[2] S. J. Trans, M. H. Devoret, H. Dai, A. Thess, R. E. Smalley, L. J. Geerligs, and C. Dekker, Nature (London) **386**, 474 (1997).
[3] A. Thess, R. Lee, P. Nikolaev, H. Dai, P. Petit, J. Robert, C. Xu, Y. H. Lee, S. G. Kim, A. G. Rinzler, D. T. Colbert, G. E. Scuseria, D. Tomanek, J. E. Fisher, and R. E. Smalley, Science **273**, 483 (1996).
[4] A. M. Rao, E. Richter, S. Bandow, B. Chase, P. C. Eklund, K. A. Williams, S. Fang, K. R. Subbaswamy, M. Menon, A. Thess, R. E. Smalley, G. Dresselhaus, and M. S. Dresselhaus, Science **275**, 187 (1997).
[5] J. M. Cowley, P. Nikolaev, A. Thess, and R. E. Smalley, Chem. Phys. Lett. **265**, 379 (1997).
[6] S. Iijima, Nature (London) **354**, 56 (1991).
[7] T. W. Ebbesen and P. M. Ajayan, Nature (London) **358**, 220 (1992).
[8] Z. G. Li, P. J. Fagan, and L. Liang, Chem. Phys. Lett. **207**, 148 (1993).
[9] X. F. Zhang, X. B. Zhang, G. Van Tendeloo, S. Amelinckx, M. Op de Beeck, and J. Van Landuyt, J. Cryst. Growth **130,** 368 (1993).
[10] D. Bernaerts, M. Op de Beeck, S. Amelinckx, J. Van Landuyt, and G. Van Tendeloo, Philos. Mag. A **74**, 723 (1996).
[11] S. Iijima and T. Ichihashi, Nature (London) **363**, 603 (1993).
[12] X. B. Zhang, X. F. Zhang, S. Amelinckx, G. Van Tendeloo, and J. Van Landuyt, Ultramicroscopy **54**, 237 (1994).
[13] L. C. Quin, J. Mater. Res. **9**, 2450 (1994).
[14] A. A. Lucas, V. Bruyninckx, and Ph. Lambin, Europhys. Lett. **35**, 355 (1996).
[15] W. Cochran, F. H. C. Crick, and V. Vand, Acta Crystallogr. **5**, 581 (1952).
[16] L. Margulis, P. Dluzewki, Y. Feldman, and R. Tenne, J. Microsc. **181**, 68 (1996).
[17] We use the convention defined in D. H. Robertson, D. W. Brenner, and J. W. Mintmire, Phys. Rev. B **45**, 12 592 (1992).
[18] This includes a factor of $2\pi/p_z$ that was missing in Ref. 14.
[19] M. S. Dresselhaus, G. Dresselhaus, and R. Saito, Carbon **33**, 883 (1995).
[20] X. Blase, A. Rubio, S. G. Louie, and M. L. Cohen, Europhys. Lett. **28**, 335 (1994).
[21] P. A. Doyle and P. S. Turner, Acta Crystallogr. **5**, 390 (1968).